Demonstration of a curved sidewall grating demultiplexer on silicon

Przemek J. Bock,[1,*] Pavel Cheben,[1] Jens H. Schmid,[1] Aitor V. Velasco,[2] André Delâge,[1] Siegfried Janz,[1] Dan-Xia Xu,[1] Jean Lapointe,[1] Trevor J. Hall,[3] and María L. Calvo[2]

[1]*Institute for Microstructural Sciences, National Research Council Canada, Ottawa, Canada*
[2]*Complutense University of Madrid, Madrid, Spain*
[3]*Centre for Research in Photonics, University of Ottawa, Ottawa, Canada*
[*]*przemek.bock@sympatico.ca*

Abstract: We experimentally demonstrate a new type of waveguide multiplexer device designed for silicon photonics, with a crosstalk level as low as −35 dB and an operational wavelength range of 300 nm. A compact device footprint of only 100 × 160 μm^2 offers an excellent potential for integration with other silicon nanophotonic circuits.

OCIS codes: (130.3120) Integrated optics devices; (050.1950) Diffraction gratings; (050.6624) Subwavelength structures.

References and links

1. C. R. Doerr and K. Okamoto, "Advances in silica planar lightwave circuits," J. Lightwave Technol. **24**(12), 4763–4789 (2006).
2. P. Cheben, "Wavelength dispersive planar waveguide devices: echelle gratings and arrayed waveguide gratings," *Optical waveguides: from theory to applied technologies*, M. L. Calvo and V. Lakshminarayanan, Eds. (CRC Press, 2007), 173–230.
3. A. Alduino and M. Paniccia, "Interconnects: wiring electronics with light," Nat. Photonics **1**(3), 153–155 (2007).
4. B. Jalali, "Teaching silicon new tricks," Nat. Photonics **1**(4), 193–195 (2007).
5. R. Kirchain and L. Kimerling, "A roadmap for nanophotonics," Nat. Photonics **1**(6), 303–305 (2007).
6. P. Cheben, J. H. Schmid, A. Delâge, A. Densmore, S. Janz, B. Lamontagne, J. Lapointe, E. Post, P. Waldron, and D.-X. Xu, "A high-resolution silicon-on-insulator arrayed waveguide grating microspectrometer with sub-micrometer aperture waveguides," Opt. Express **15**(5), 2299–2306 (2007).
7. F. Xia, L. Sekaric, and Y. Vlasov, "Ultracompact optical buffers on a silicon chip," Nat. Photonics **1**(1), 65–71 (2007).
8. J. S. Levy, A. Gondarenko, M. A. Foster, A. C. Turner-Foster, A. L. Gaeta, and M. Lipson, "CMOS-compatible multiple-wavelength oscillator for on-chip optical interconnects," Nat. Photonics **4**(1), 37–40 (2010).
9. H. A. Rowland, "Preliminary notice of results accomplished on the manufacture and theory of gratings for optical purposes," Phil. Mag. Suppl. **13**(84), 469–474 (1882).
10. R. Nagarajan, M. Kato, J. Pleumeekers, P. Evans, S. Corzine, S. Hurtt, A. Dentai, S. Murthy, M. Missey, R. Muthiah, R. A. Salvatore, C. Joyner, R. Schneider, M. Ziari, F. Kish, and D. Welch, "InP Photonic Integrated Circuits," IEEE J. Sel. Top. Quantum Electron. **16**(5), 1113–1125 (2010).
11. X. Leijtens and M. Smit, "Miniaturization of Passive Devices for Photonic Integration," Proc. SPIE **6020**, 60201Q (2005).
12. M. R. T. Pearson, A. Bezinger, A. Delâge, J. W. Fraser, S. Janz, P. E. Jessop, and D.-X. Xu, "Arrayed waveguide grating demultiplexers in silicon-on-insulator," Proc. SPIE **3953**, 11–18 (2000).
13. F. Ohno, K. Sasaki, A. Motegi, and T. Baba, "Reduction in Sidelobe Level in Ultracompact Arrayed Waveguide Grating Demultiplexer Based on Si Wire Waveguide," Jpn. J. Appl. Phys. **45**(8A), 6126–6131 (2006).
14. P. Dumon, W. Bogaerts, D. Van Thourhout, D. Taillaert, R. Baets, J. Wouters, S. Beckx, and P. Jaenen, "Compact wavelength router based on a Silicon-on-insulator arrayed waveguide grating pigtailed to a fiber array," Opt. Express **14**(2), 664–669 (2006).
15. X. Liu, I. Hsieh, X. Chen, M. Takekoshi, J. I. Dadap, N. C. Panoiu, R. M. Osgood Jr., W. M. Green, F. Xia, and Y. A. Vlasov, "Design and fabrication of an ultra-compact silicon on insulator demultiplexer based on arrayed waveguide gratings," CLEO 2008, paper CTuNN1.
16. S. Pathak, E. Lambert, P. Dumon, D. Thourhout, and W. Bogaerts, "Compact SOI-Based AWG With Flattened Spectral Response Using a MMI," 8th International Conference in Group IV Photonics 2011, paper WC2.
17. S. Janz, A. Balakrishnan, S. Charbonneau, P. Cheben, M. Cloutier, A. Delâge, K. Dossou, L. Erickson, M. Gao, P. A. Krug, B. Lamontagne, M. Packirisamy, M. Pearson, and D.-X. Xu, "Planar waveguide echelle gratings in silica-on-silicon," IEEE Photon. Technol. Lett. **16**(2), 503–505 (2004).
18. S. Bidnyk, D. Feng, A. Balakrishnan, M. Pearson, M. Gao, H. Liang, W. Qian, C.-C. Kung, J. Fong, J. Yin, and M.

#167409 - $15.00 USD Received 27 Apr 2012; revised 24 Jul 2012; accepted 30 Jul 2012; published 15 Aug 2012

Asghari, "Silicon-on-insulator-based planar circuit for passive optical network applications," IEEE Photon. Technol. Lett. **18**(22), 2392–2394 (2006).
19. J. Brouckaert, W. Bogaerts, P. Dumon, D. Thourhout, and R. Baets, "Planar concave grating demultiplexer fabricated on a nanophotonic silicon-on-insulator platform," J. Lightwave Technol. **25**(5), 1269–1275 (2007).
20. D. Feng, N.-N. Feng, C.-C. Kung, H. Liang, W. Qian, J. Fong, B. J. Luff, and M. Asghari, "Compact single-chip VMUX/DEMUX on the silicon-on-insulator platform," Opt. Express **19**(7), 6125–6130 (2011).
21. K. Okamoto, "Fundamentals of optical waveguides," Elsevier Inc., 2006.
22. R. Soref, "Reconfigurable integrated optoelectronics," Adv. Optoelectron. **2011**, 1–15 (2011), doi:10.1155/2011/627802.
23. F. Xia, M. Rooks, L. Sekaric, and Y. Vlasov, "Ultra-compact high order ring resonator filters using submicron silicon photonic wires for on-chip optical interconnects," Opt. Express **15**(19), 11934–11941 (2007).
24. N. Han-Yong, R. W. Michael, L. Daqun, W. Xuan, M. Jose, R. P. Roberto, and P. Kachesh, "4 x 4 wavelength reconfigurable photonic switch based on thermally tuned silicon microring resonators," Opt. Eng. **47**(4), 0446011–0666018 (2008).
25. N. Sherwood-Droz, H. Wang, L. Chen, B. G. Lee, A. Biberman, K. Bergman, and M. Lipson, "Optical 4x4 hitless slicon router for optical networks-on-chip (NoC)," Opt. Express **16**(20), 15915–15922 (2008).
26. X. Zheng, I. Shubin, G. Li, T. Pinguet, A. Mekis, J. Yao, H. Thacker, Y. Luo, J. Costa, K. Raj, J. E. Cunningham, and A. V. Krishnamoorthy, "A tunable 1x4 silicon CMOS photonic wavelength multiplexer/demultiplexer for dense optical interconnects," Opt. Express **18**(5), 5151–5160 (2010).
27. Y. H. Wen, O. Kuzucu, T. Hou, M. Lipson, and A. L. Gaeta, "All-optical switching of a single resonance in silicon ring resonators," Opt. Lett. **36**(8), 1413–1415 (2011).
28. C. K. Madsen, J. Wagener, T. A. Strasser, D. Muehlner, M. A. Milbrodt, E. J. Laskowski, and J. DeMarco, "Planar waveguide optical spectrum analyzer using a UV-induced grating," IEEE J. Sel. Top. Quantum Electron. **4**(6), 925–929 (1998).
29. Y. Hao, Y. Wu, J. Yang, X. Jiang, and M. Wang, "Novel dispersive and focusing device configuration based on curved waveguide grating (CWG)," Opt. Express **14**(19), 8630–8637 (2006).
30. P. J. Bock, P. Cheben, A. Delâge, J. H. Schmid, D.-X. Xu, S. Janz, and T. J. Hall, "Demultiplexer with blazed waveguide sidewall grating and sub-wavelength grating structure," Opt. Express **16**(22), 17616–17625 (2008).
31. C. F. R. Mateus, M. C. Y. Huang, L. Chen, C. J. Chang-Hasnain, and Y. Suzuki, "Broad-band mirror (1.12-1.62 um) using a subwavelength grating," IEEE Photon. Technol. Lett. **16**(7), 1676–1678 (2004).
32. P. Cheben, D.-X. Xu, S. Janz, and A. Densmore, "Subwavelength waveguide grating for mode conversion and light coupling in integrated optics," Opt. Express **14**(11), 4695–4702 (2006).
33. P. Cheben, P. J. Bock, J. H. Schmid, J. Lapointe, S. Janz, D.-X. Xu, A. Densmore, A. Delâge, B. Lamontagne, and T. J. Hall, "Refractive index engineering with subwavelength gratings for efficient microphotonic couplers and planar waveguide multiplexers," Opt. Lett. **35**(15), 2526–2528 (2010).
34. R. Halir, P. Cheben, J. H. Schmid, R. Ma, D. Bedard, S. Janz, D.-X. Xu, A. Densmore, J. Lapointe, and I. Molina-Fernández, "Continuously apodized fiber-to-chip surface grating coupler with refractive index engineered subwavelength structure," Opt. Lett. **35**(19), 3243–3245 (2010).
35. U. Levy, M. Abashin, K. Ikeda, A. Krishnamoorthy, J. Cunningham, and Y. Fainman, "Inhomogenous Dielectric Metamaterials with Space-Variant Polarizability," Phys. Rev. Lett. **98**(24), 243901 (2007).
36. J. H. Schmid, P. Cheben, S. Janz, J. Lapointe, E. Post, and D.-X. Xu, "Gradient-index antireflective subwavelength structures for planar waveguide facets," Opt. Lett. **32**(13), 1794–1796 (2007).
37. F. Horst, W. M. Green, B. J. Offrein, and Y. Vlasov, "Echelle grating WDM (de-)multiplexer in SOI technology, based on a design with two stigmatic points," Proc. SPIE **6996**, 69960R, (2008).

1. Introduction

Presently, two types of passive waveguide multiplexer and router technologies, namely array waveguide gratings and echelle gratings, are used as fundamental building blocks for wavelength division multiplexed communications [1,2]. Although remarkable progress has been achieved in these complex integrated optical circuits, with applications recently extending from telecom to optical interconnects [3–5] and spectroscopy [6], the best performance is still achieved using conventional glass waveguide technology. While multiplexer optical quality remains unrivalled in silica glass waveguides, such devices are several orders of magnitude larger than multiplexers based on silicon nanophotonic waveguides. With advanced silicon nanophotonic components rapidly emerging, including optical memories, buffers [7] and light sources [8], small footprint multiplexers are a key component in the commercial realization of silicon photonic circuit technology.

Planar waveguide multiplexers use a wavelength dispersive element to spatially separate different spectral bands. Such a dispersive element is implemented in a focusing geometry to collect the light of different wavelengths by an array of receiver waveguides located along the focal curve, constructed according to a geometry which minimizes wavefront aberrations,

#167409 - $15.00 USD Received 27 Apr 2012; revised 24 Jul 2012; accepted 30 Jul 2012; published 15 Aug 2012

discovered by Henry Rowland in the late 19th century [9]. The wavelength dispersive element used in an array waveguide grating (AWG) is the waveguide phased array, with a linearly increasing waveguide length across adjacent arms of the array. The waveguide array is often the single largest component of an AWG multiplexer and its phase errors limit the device performance in terms of crosstalk between different wavelength channels. A crosstalk level of −35 dB or less can be achieved in a glass AWG. Nevertheless, the large minimum bend radius of glass waveguides inevitably leads to large devices, on the order of several centimetres in size, not suitable for integration. Complex photonic integrated circuits with AWGs [10,11] were successfully built and commercialized for telecom applications using the InP waveguide platform, but no similar integration level has yet been achieved in silicon waveguides. Recently, several ultra-compact AWG multiplexers have been reported using the silicon-on-insulator high refractive index contrast (Δn ~2) material platform [12–16]. However, in such high-index-contrast waveguides, the light intensity at the core-cladding boundary is substantially increased. Normal manufacturing variations will interact with this field, resulting in an overall phase error accumulation, ultimately limiting the crosstalk performance. Conversely, the dispersive element in an echelle multiplexer is the etched waveguide grating [2,17]. Several echelle grating multiplexers have been recently reported using silicon photonic waveguides [18–20]. Operating in reflection, the efficiency and bandwidth of these devices are restricted by limited reflectivity of the etched grating facets. Furthermore, the facet reflectivity cannot be controlled (apodized) along the grating without incurring additional loss, while such apodization capability is required for advanced multiplexers with controlled passband and chromatic dispersion.

A great deal of research has been done in developing both passive and reconfigurable integrated filters [21,22]. Here we propose a new type of passive wavelength multiplexer for silicon. Silicon photonic devices have many advantages including possible low cost fabrication due to the potential compatibility with the microelectronics fabrication infrastructure, high integration potential and fabrication yield. Besides AWGs and Echelle gratings, cascaded Mach-Zehnder interferometers and ring resonator filters have been proposed [23]; however, both require exact optical path lengths and are highly sensitive to fabrication tolerance. Reconfigurable ring filters do not have this limitation, but do require an active tuning element [24–27]. Another alternative is channel waveguide gratings, which were first implemented in straight waveguides using UV induced gratings as the dispersive element while either chirping the grating [28] or curving the waveguide [29] provides the focusing property.

2. Demultiplexer operating principle

In this letter we experimentally demonstrate a new type of passive multiplexer device, which has been specifically designed for course wavelength division multiplexing (CWDM) on the silicon-on-insulator (SOI) material platform. In our demultiplexer, the dispersive element is the waveguide sidewall grating, where the light in the input waveguide is preferentially diffracted towards the focal curve by 45° blazed grating teeth. Conceptually, the light is being reflected by total internal reflection at the grating facet, where each grating tooth behaves like a small prism, thereby increasing grating diffraction efficiency into the −1st order compared to the 1st order. As the light propagates along the waveguide, each tooth acts as a Huygens wavelet source, partially dispersing the light.

The device properties can be estimated using the relationship between the grating tooth spacing and the incident and diffractive angle - the well-known grating equation. In our case, it simplifies to $\Lambda(1 + \sin\varphi_d) = m\ \lambda/n_{eff}$, where $\Lambda = |m\lambda_o/n_{eff}|$ is the grating pitch, λ_o is the center wavelength, n_{eff} is the effective index of the waveguide grating and φ_d is the diffraction angle relative to the grating. The angular dispersion is then $\Delta\varphi_d/\Delta\lambda = -m/(n_{eff}d\cos\varphi_d)$ and at $\varphi_d = 0$, becomes $\Delta\varphi_d/\Delta\lambda = 1/\lambda_o$. Likewise, the free spectral range (FSR) is $\Delta\varphi_d/\Delta m = \lambda/(n_{eff}d\cos\varphi_d)$ and at $\varphi_d = 0$ becomes $\Delta\varphi_d/\Delta m = 1/m$. Note that unlike an AWG or echelle grating, the dispersion is

#167409 - $15.00 USD Received 27 Apr 2012; revised 24 Jul 2012; accepted 30 Jul 2012; published 15 Aug 2012

independent of the order (pitch) of the grating. Therefore, to design a version of this device for dense wavelength division multiplexing (DWDM), the Rowland radius would need to be scaled accordingly to accommodate more receiver waveguides along the focal curve.

These properties are confirmed by using a 2D Kirchhoff-Huygens diffraction integral to model the device as shown in Eq. (1), where the far-field $\Psi(x', y')$ at coordinates x' and y' along the focal curve (the Rowland circle of radius R) is calculated by integrating the near-field along the curved grating path $C(x,y)$.

$$\Psi(x', y') = \int_C \frac{\psi(x, y) \exp[-i(\phi_w + \phi_s)]}{\sqrt{\lambda d}} G dC \tag{1}$$

The near-field profile is defined as $\psi(x, y)$ at coordinates x and y along the grating, The phase accumulated in the grating waveguide and in the slab region by the Huygens wavelet is φ_w, φ_s. In Eq. (1), λ is the wavelength, $d = [(x'- x)^2 + (y'- y)^2]^{1/2}$ is the distance between a grating facet (at x,y) and a given position along the focal curve (at x', y'), and the geometry factor is $G = (\cos\alpha + \cos\gamma)/2$, where α and γ are the angles between the normal of the grating facet and the incoming and outgoing light wavevector respectively. In Eq. (1) each grating facet is represented as a wavelet source, and the relative phase between sources is fixed. The facets shape the profile of the electromagnetic field near the grating, while the curvature of the waveguide focuses the wavefront onto the focal curve, where the light is intercepted by the receiver waveguides. For our device, the discretized Kirchhoff-Huygens diffraction integral, i.e. sum of light contribution from all facets $j = 1,2, \ldots, N$ was used in our preview study to model the device [30]. This model is summarized in Fig. 1, where the near-field along the N facets of the grating is integrated at each point along the focal curve.

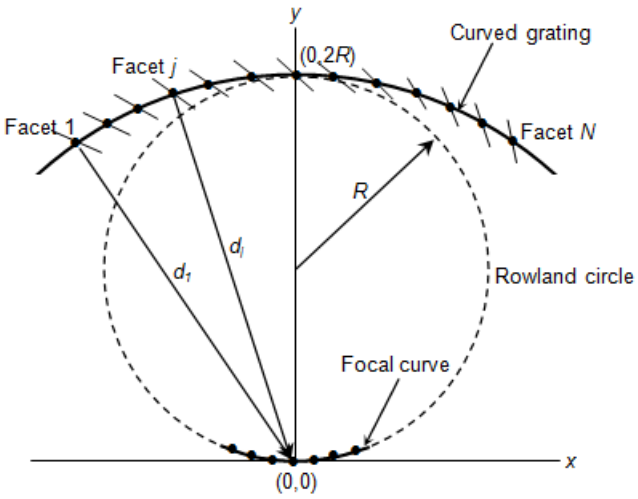

Fig. 1. Schematic of the discretized Kirchhoff-Huygens model of the sidewall grating spectrometer with N facets having a Roland radius of R. Coordinates x, y are relative to the focal curve.

Conventional passive multiplexers including AWGs (and echelle gratings) use a split-path approach, dividing the light between the array waveguides (gratings). For a given split-path, a particular array waveguide in an AWG for example, the light accumulates phase errors independent of other array waveguides. This leads to a large phase error accumulation relative to an adjacent array waveguide, even though the length different between adjacent array waveguides is only the order spacing. A key element of our design is the light propagates along the common-path of the curved sidewall grating. Therefore, unlike the split-path approach, the

#167409 - $15.00 USD Received 27 Apr 2012; revised 24 Jul 2012; accepted 30 Jul 2012; published 15 Aug 2012

common-path approach results in a dependent phase error accumulation between adjacent grating facets. For example, the phase error accumulation between facet j and facet $j + 1$ only includes the order spacing between adjacent facets as the phase error accumulated up to facet j is common to both facet j and facet $j + 1$. The schematic in Fig. 2(a) shows the conventional split-path multiplexing approach used in an AWG where φ_1, φ_j, φ_{j+1} and φ_N are the phase errors accumulated along the first, j^{th}, $j^{th} + 1$ and N^{th} array waveguide (N is the total number of array waveguides). The relative phase error between the j^{th} and the $j^{th} + 1$ array waveguide is $\Delta\varphi = \varphi_{j+1} - \varphi_j$, since phase error is accumulated independently between the different array waveguides. Figure 2(b) shows a schematic of the common-path multiplexing approach used in the sidewall grating. Since the light propagates along a common path, the relative phase error between adjacent facets is $\Delta\varphi = \varphi_{j+1} - \varphi_j = (\Delta\varphi_{j,j+1} + \varphi_j) - \varphi_j = \Delta\varphi_{j,j+1}$, where $\Delta\varphi_{j,j+1}$ is the phase error accumulation between facet j and facet $j + 1$. This is theoretically a significant advantage because the phase error accumulation between adjacent facets is limited to only a single order spacing.

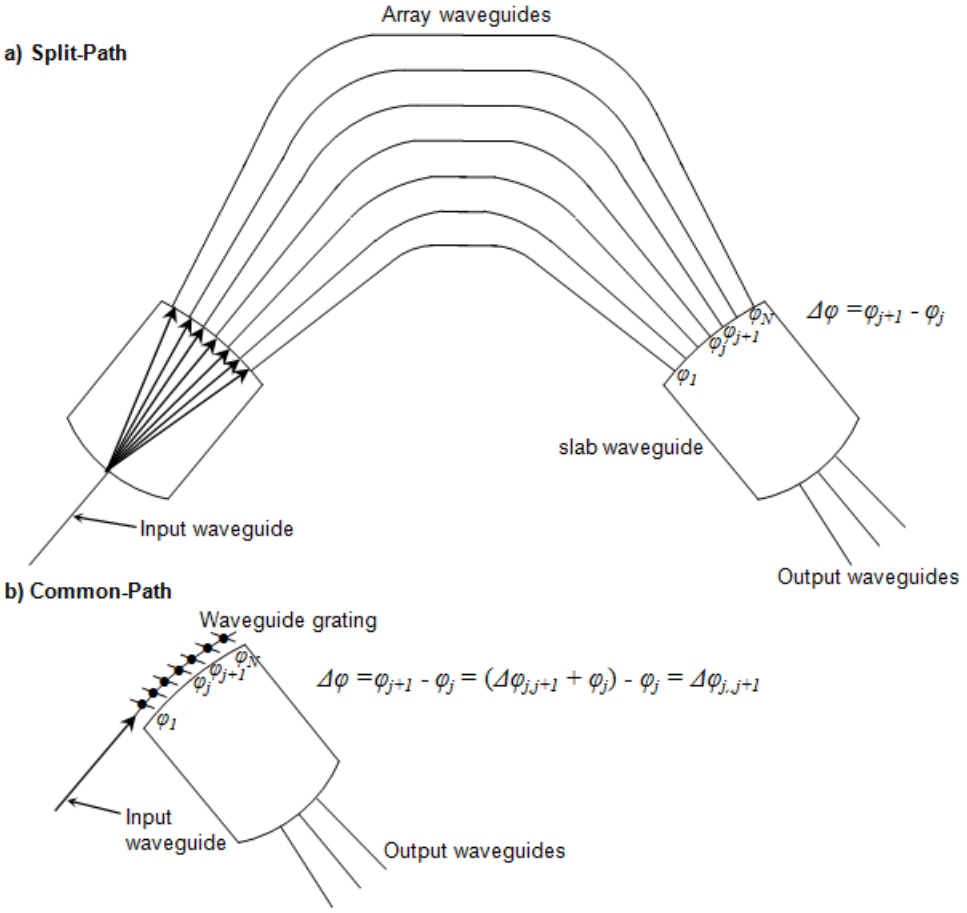

Fig. 2. a) Schematic of the conventional split-path multiplexing approach used in an AWG where φ_1, φ_j, φ_{j+1} and φ_N are the phase errors accumulated along the first, j^{th}, $j^{th} + 1$ and N^{th} array waveguide (N is the total number of array waveguides). The relative phase error between the j^{th} and the $j^{th} + 1$ array waveguide is $\Delta\varphi = \varphi_{j+1} - \varphi_j$, since phase error is accumulated independently between the different array waveguides. b) Schematic of the common-path multiplexing approach used in the sidewall grating. Since the light propagates along a common path, the relative phase error between adjacent facets will be $\Delta\varphi = \varphi_{j+1} - \varphi_j = (\Delta\varphi_{j,j+1} + \varphi_j) - \varphi_j = \Delta\varphi_{j,j+1}$, where $\Delta\varphi_{j,j+1}$ is the phase error accumulation between facet j and facet $j + 1$.

#167409 - $15.00 USD Received 27 Apr 2012; revised 24 Jul 2012; accepted 30 Jul 2012; published 15 Aug 2012

3. Design and fabrication

The geometry of the Rowland configuration was determined as follows. At the Rowland circle, the receiver waveguide width and pitch of 1.4 μm and 2.4 μm respectively, were chosen to ensure compact size yet avoid mode delocalization and minimize receiver-limited crosstalk. For such a receiver waveguide, the numerical aperture angular full width is 40.1° from 3D FDTD simulations, measured at $1/e^2$ irradiance asymptotes. For a L = 100 μm long curved sidewall grating, 40.1° angular width corresponds to a focal length of f = 140 μm, thus a Rowland circle radius of R = 70 μm. This geometry ensures that the numerical aperture of the receiver waveguides is matched to the numerical aperture of the curved waveguide grating equivalent lens.

For the 21-channel device, the sidewall grating pitch is $\Lambda = |m\lambda_o/n_{eff}| = 0.512$ μm, where $m = -1$ is the grating order, $\lambda_0 = 1.44$ μm is the center wavelength and $n_{eff} = 2.81$ is the effective index of the curved waveguide for TE polarization. For the two-pass filter created by cascading two 11-channel devices, the sidewall grating pitch is $\Lambda = |m\lambda_o/n_{eff}| = 0.561$ μm, where $m = -1$, $\lambda_0 = 1.55$ μm and $n_{eff} = 2.76$. Effective index was determined by using a FDTD mode solver for a 0.6 μm × 0.26 μm silicon waveguide ($n_{Si} = 3.476$) on a silica substrate ($n_{SiO2} = 1.444$) with an SU-8 cladding ($n_{SU-8} = 1.58$). The apodized grating has an initial modulation depth of 0.03 μm, which increases to the maximum depth of 0.3 μm over the first 70 μm of the grating. The apodization function is $d = d_0\exp(-x^2/2\sigma^2)$, where d_0 is twice the maximum modulation depth, x is the position along the grating and σ = 60 μm is the variance of the Gaussian function. Maximum grating depth (0.3 μm) is used for the remaining 30 μm of grating length. The grating pitch varies according to the modulation depth by $\delta\Lambda = d^2(n_{Si} - n_{SU8})/2wn_{Si}$, where $\delta\Lambda$ is the required change in pitch, d is the modulation depth, w = 0.6 μm is the waveguide width and n_{Si}, n_{SU8} are the refractive indices of silicon and SU-8 polymer. These parameters result in a curved waveguide with 183 blazed grating teeth. Triangular subwavelength grating nanostructure with a 1 μm width and a 0.25 μm pitch was used as a transition between the waveguide grating and the slab waveguide, resulting in a total of 400 subwavelength grating periods.

We used commercially available SOI substrates with 0.26-μm-thick silicon and 2-μm-thick buried oxide (BOX) layers. Electron beam lithography was used to define the waveguide layout in high contrast hydrogen silsesquioxane (HSQ) resist, which formed SiO_2 upon electron beam exposure. We used inductively coupled plasma reactive ion etching (ICP-RIE) to transfer the waveguide layout onto the silicon layer. Samples were coated with a 2 μm thick polymer (SU-8, n_{SU-8} ~1.58 at λ = 1.55 μm), then cleaved into separate chips and facets polished. Chips were approximately 6.1 mm long. Figure 3(a) shows an optical microscope image of the fabricated 21-channel spectrometer, while Fig. 3(b) shows a scanning electron microscope close-up of the grating detail. Scanning electron microscope images showed a 50 nm offset from the desired dimensions, which we attribute to insufficient correction of the proximity effect.

#167409 - $15.00 USD Received 27 Apr 2012; revised 24 Jul 2012; accepted 30 Jul 2012; published 15 Aug 2012

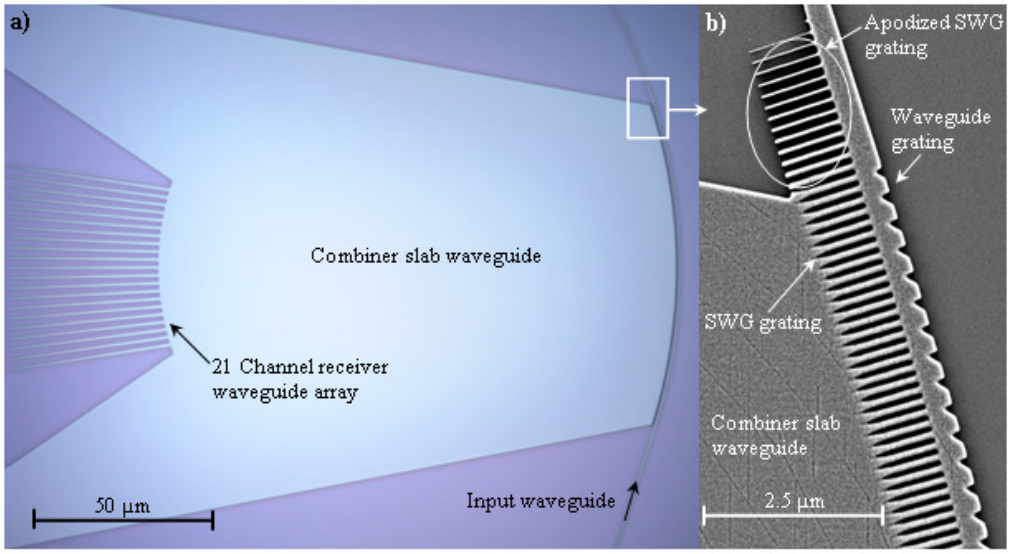

Fig. 3. a) Optical image of the sidewall grating spectrometer showing the input waveguide and the 21-channel output receiver waveguide array. b) Scanning electron microscope image close-up of the blazed waveguide grating and subwavelength grating (SWG) nanostructure detail.

4. Experimental results

A polarization controller with a broadband tunable external cavity semiconductor laser (Santec) was used to measure transmission spectra (λ = 1.23 – 1.63 µm). To couple the light into the chip, we used a lensed fiber resulting in a Gaussian beam waist of ~2 µm and an on-chip subwavelength grating fiber-chip coupler. Light is coupled out of the chip using an identical subwavelength grating coupler and subsequently focused by a microscope objective lens onto an InGaAs photodetector. The intrinsic loss of the device was measured with test multiplexers designed to calibrate out waveguide propagation loss and input/output coupling loss in the intrinsic loss measurement.

For efficient coupling to the receiver waveguides, the field distribution at the focal curve must match the modal field of the output receiver waveguide. Since the mode profile of a waveguide is nearly Gaussian, a Gaussian distribution in the grating near-field is required to ensure the far-field matching condition at the focal curve. This is achieved by apodizing the depth of the sidewall grating teeth to reshape an exponential diffracted near-field into a Gaussian diffraction profile, while simultaneously minimizing back-reflections by creating a smooth transition from the waveguide to the waveguide grating. The apodization function used is $d = d_0\exp(-x^2/2\sigma^2)$, where d_0 is the maximum grating modulation depth, x is the position along the grating and σ is the variance of the Gaussian function. Once the maximum grating modulation depth is reached, a constant grating modulation depth interacts with the diminished waveguide mode intensity to create the tail of the field profile diffracted near the end of the grating. Figure 4(a) shows a comparison of the spectra between the nominal apodized spectrometer (grey curves), and a test spectrometer (coloured curves) without the apodization for a constant grating modulation depth of 300 nm, indicating significantly reduced loss and crosstalk for the nominal design.

#167409 - $15.00 USD Received 27 Apr 2012; revised 24 Jul 2012; accepted 30 Jul 2012; published 15 Aug 2012

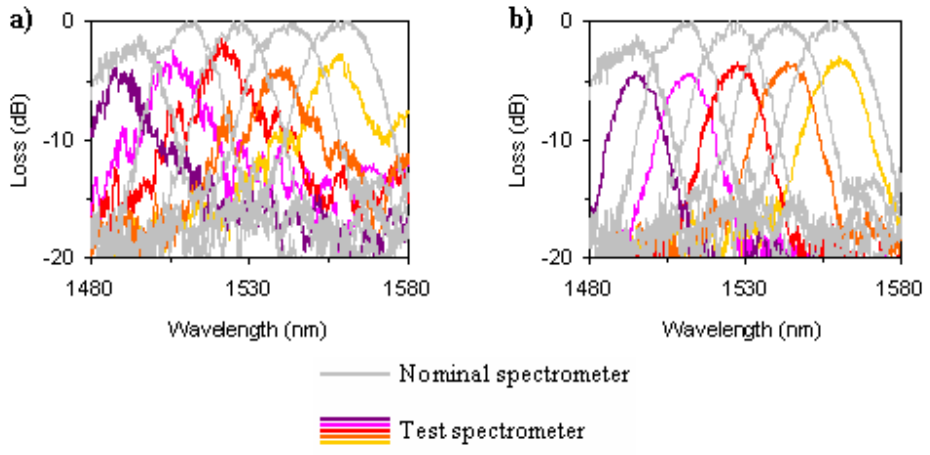

Fig. 4. Comparison of the transmission spectra for TE polarization between a nominal (apodized and chirped) spectrometer (grey) and a test spectrometer (colored) a) without apodization for a constant modulation depth of 300 nm, indicating poor crosstalk performance and b) without the subwavelength anti-reflective nanostructure, indicating a 4 dB loss penalty.

However, varying the modulation depth of the grating produces a corresponding change in the effective index of each grating segment, resulting in a phase-front distortion and a broadening of the far-field [30]. We eliminated the phase-front errors by chirping the grating to ensure a constant effective index for the entire length of the apodized grating. A simple geometric relation was used to calculate the required compensatory chirp for a given modulation depth, namely $\delta\Lambda = d^2(n_{Si} - n_{SU8})/2wn_{Si}$ from the previous section. The validity of this relation was confirmed by finite-difference time-domain (FDTD) simulations [30]. The ability to use apodization and chirping to control both the amplitude and the phase of the near-field profile facilitates freedom in tailoring the device pass-band and chromatic dispersion [2]. In existing technologies like echelle gratings, no efficient method to control the field amplitude distribution is known (it would require varying the reflectivity of the echelle facets, leading to loss), while in an AWG this would demand either gain or attenuation in the waveguide phased array.

Fundamental to the operation of our sidewall grating multiplexer is a subwavelength nanostructure between the sidewall grating waveguide and the slab waveguide. Such a nanostructure provides confinement to ensure the channel waveguide with the sidewall grating supports a fundamental transverse mode, while simultaneously acting as a transparent waveguide boundary in the direction normal to the channel waveguide, which results in efficient coupling to the slab waveguide. Subwavelength high-index contrast gratings were first proposed as high-reflectivity mirrors [31] fiber-chip couplers [32–34] and lenses [35]. While subwavelength gratings have been used as a cladding in silicon waveguides, anti-reflective structures [36,37] and planar waveguides, this is the first demonstration of their threefold use: acting simultaneously as a waveguide cladding, an anti-reflective boundary and a slab waveguide. Our device uses 400 periods of the subwavelength nanostructure between the grating waveguide and the combiner slab waveguide. The effect of the subwavelength nanostructure is shown in Fig. 4(b) by comparing the spectral response of the nominal spectrometer (with the nanostructure) to a test spectrometer with a 1-μm-wide trench between the waveguide grating and the slab waveguide. By using the subwavelength grating, there is a remarkable 4 dB loss reduction indicating that this nanostructure facilitates efficient transitions between very different waveguide geometries, even in a high refractive index contrast material platform such as SOI. Our subwavelength nanostructures were apodized on both ends of the

#167409 - $15.00 USD Received 27 Apr 2012; revised 24 Jul 2012; accepted 30 Jul 2012; published 15 Aug 2012

blazed sidewall grating to prevent Fresnel reflections as the mode couples from the input waveguide to the waveguide grating section, as shown in Fig. 3(b).

The spectral response of the multiplexer is shown in Fig. 5 indicating a crosstalk of 20-25 dB with a channel spacing of $\Delta\lambda$ = 15 nm over a wavelength range of λ = 1330 – 1630 nm. Using specifically designed test multiplexers, an intrinsic device loss (including diffraction loss, coupling loss from the waveguide grating to the slab waveguide and excess loss due to field mismatch at receiver waveguides) is measured to be 3-4 dB. Reduction in performance at short wavelengths is a result of approaching the band gap of our subwavelength grating fiber-chip coupler [33]. Compared to other microphotonic multiplexers [13–16], our device has better crosstalk performance (compared with 13 dB [13], 12 dB [14], 5-10 dB [15], and 17 dB crosstalk [16]) and a far broader operational bandwidth of 300 nm (compared with 140 nm [13], 30 nm [14], 1.5 nm [15], and 40 nm bandwidth [16]). The device footprint is only 100 × 160 μm^2 making it one of the smallest wavelength multiplexers. Since the device is so small, it can easily be cascaded to form a two-pass wavelength filter as shown in the optical image in Fig. 6.

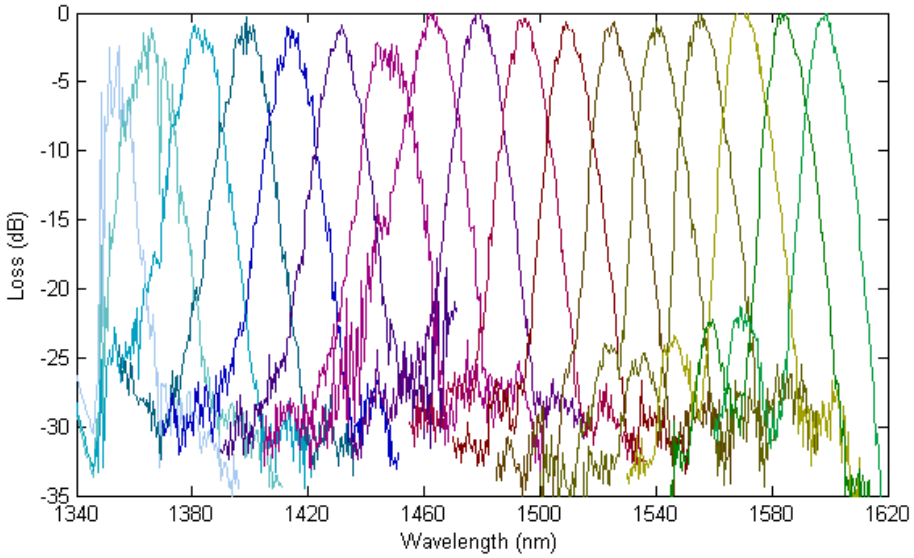

Fig. 5. Transmission spectrum of the nominal spectrometer for TE polarization for a wavelength range of λ = 1340 – 1620 nm.

#167409 - $15.00 USD Received 27 Apr 2012; revised 24 Jul 2012; accepted 30 Jul 2012; published 15 Aug 2012

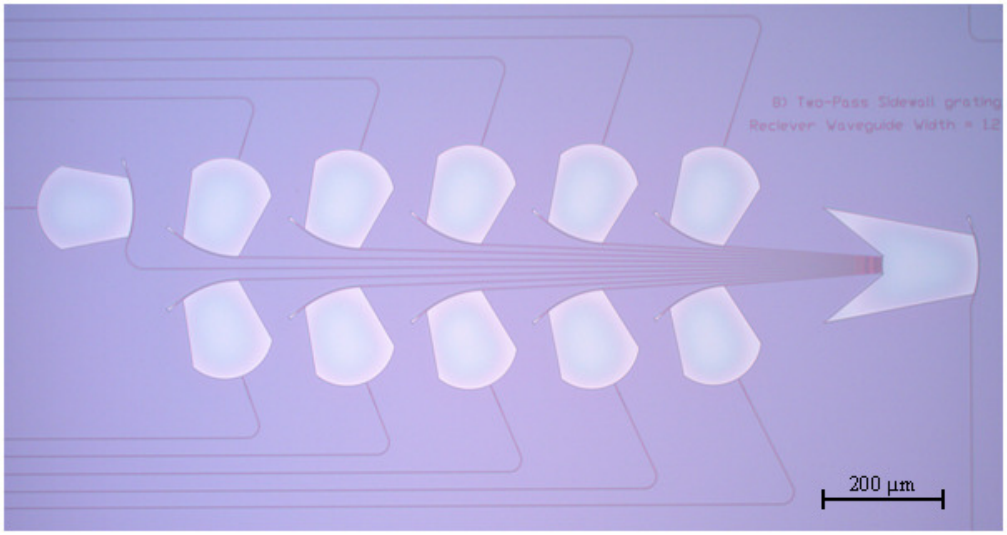

Fig. 6. Optical image of the two-pass spectral filter formed by cascading two 11 channel sidewall grating spectrometers.

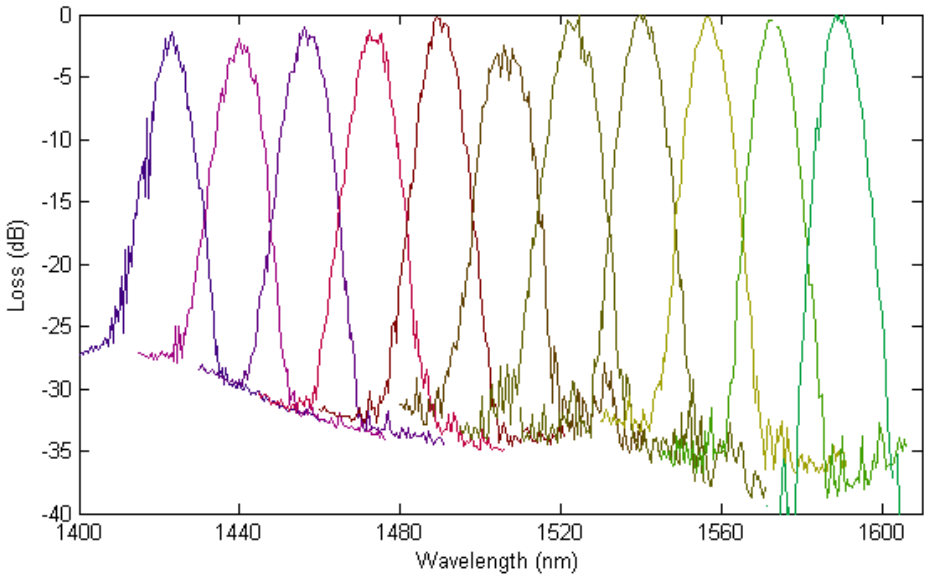

Fig. 7. Transmission spectrum of the two-pass spectrometer for a wavelength range of λ = 1400 – 1600 nm (TE polarization).

The input light is first spectrally filtered by an 11 channel multiplexer and subsequently passes through another identical device with a single receiver waveguide for the specific wavelength channel. To minimize connectivity complexity, we terminated the multiplexer blazed grating waveguides with a taper (width 0.6 µm to 5 µm) to expand the waveguide mode into a SWG anti-reflection structure, to divert any residual light away from the output facet of the chip. Figure 7 shows the spectral response of the two-pass multiplexer indicating an excellent crosstalk performance reaching −35 dB at longer wavelengths (1560 – 1600 nm). Some increase in the noise floor at short wavelengths appears to be caused by approaching the fiber-to-chip SWG coupler band gap [19]. This can be avoided by selecting a shorter

#167409 - $15.00 USD Received 27 Apr 2012; revised 24 Jul 2012; accepted 30 Jul 2012; published 15 Aug 2012

periodicity for SWG coupler to move its band gap outside the short wavelength range of the sidewall grating spectrometer.

Our multiplexer channel spacing is targeting course wavelength division for interconnect applications. To accommodate the dense wavelength division of telecommunication applications, our device would need to be upscaled by a factor of $\Delta\lambda/\Delta\lambda_{DWDM}$ ~19 for a spacing of 100 GHz.

5. Conclusion

These results suggest that the sidewall grating multiplexer can achieve comparable performance to established technologies such as AWGs and echelle gratings. In particular the very small size, the low crosstalk, the broadband operation and the freedom in pass-band tailoring lend themselves well to promising applications in optical interconnects. Specifically, the small footprint combined with the large operation bandwidth is a possible solution for coarse wavelength division multiplexing. Theoretically, our device minimizes phase error accumulation by implementing a common-path approach.

These results also suggest that subwavelength nanostructures can be advantageously used in demultiplexing planar waveguide circuits to simultaneously provide multiple functions including anti-reflection, coupling from grating waveguide to slab waveguide and confinement of the waveguide grating mode. The subwavelength nanostructures provide an excellent means to engineer materials with different effective refractive indexes not limited to those typically used in silicon-based microfabrication process, simply by changing the nanostructure geometry.

#167409 - $15.00 USD Received 27 Apr 2012; revised 24 Jul 2012; accepted 30 Jul 2012; published 15 Aug 2012